Symmetry Breaking in Nanostructure Development of Carbogenic Molecular Sieves: Effects of Morphological Pattern Formation on Oxygen and Nitrogen Transport

ARTICLE *in* CHEMISTRY OF MATERIALS · AUGUST 1996

Impact Factor: 8.35 · DOI: 10.1021/cm960085w

3 AUTHORS, INCLUDING:

Henry C Foley
University of Missouri
201 PUBLICATIONS **3,389** CITATIONS

SEE PROFILE

Symmetry Breaking in Nanostructure Development of Carbogenic Molecular Sieves: Effects of Morphological Pattern Formation on Oxygen and Nitrogen Transport

Michael S. Kane, Jesse F. Goellner, and Henry C. Foley*

Center for Catalytic Science and Technology, Department of Chemical Engineering, University of Delaware, Newark, Delaware 19716

Remo DiFrancesco and Simon J. L. Billinge

Department of Physics and Astronomy, Michigan State University, East Lansing, Michigan 48224

Lawrence F. Allard

High Temperature Materials Laboratory, Oak Ridge National Laboratory, Oak Ridge, Tennessee 37831

Received February 1, 1996. Revised Manuscript Received May 1, 1996[⊗]

A comprehensive study has been undertaken to establish the primary factors that control transport of oxygen and nitrogen in polymer-derived carbogenic molecular sieves (CMS). Characterization of the nanostructure of CMS derived from poly(furfuryl alcohol) (PFA) indicates that significant physical and chemical reorganization occurs as a function of synthesis temperature. Spectroscopic measurements show a drastic decrease in oxygen and hydrogen functionality with increasing pyrolysis temperature. Structural reorganization and elimination of these heteroatoms lead to a measurable increase in the unpaired electron density in these materials. High-resolution transmission electron microscopy and powder neutron diffraction are used to probe the corresponding changes in the physical structural features in the CMS. These indicate that as the pyrolysis temperature is increased, the structure of the CMS transforms from one that is disordered and therefore highly symmetric to one that is more ordered on a length scale of 15 Å and hence less symmetric. This structural transformation process, one of symmetry breaking and pattern formation, is often observed in other nonlinear dissipative systems, but not in solids. Symmetry breaking provides the driving force for these high-temperature reorganizations, but unlike most dissipative systems, these less-symmetric structures remain frozen in place when energy is no longer applied. The impact of these nanostructural reorganizations on the molecular sieving character of the CMS is studied in terms of the physical separation of oxygen and nitrogen. These results show that the effective diffusivities of oxygen and nitrogen in the CMS vary by more than an order of magnitude across the range of synthesis temperatures studied. Although the electronic nature of the CMS leads to higher equilibrium capacity for oxygen, it is the physical nanostructure which governs the separation of these two molecules. It is concluded that the primary separation mechanism is steric and configurational in nature, a conclusion in good agreement with the general features of the kinetic hypothesis conjectured by earlier workers.

Introduction

Small-molecule transport control in molecular sieve materials is an essential element of rational advanced adsorbent and catalyst design. This goal motivates, for example much of the recent research aimed at structure-directed synthesis and computational modeling of zeolites. Molecular discrimination between species on the basis of size, shape, and heat of adsorption has been a primary feature of zeolites, especially since they can be varied through ion exchange, framework substitution, or changes in structural type.[1−3] A notable example of this approach is the recovery of oxygen from air over lithium-exchanged zeolite A. Because of its quadrupole moment, nitrogen is more strongly adsorbed than oxygen on the zeolite surface.[4,5] As a result, the oxygen is transported through the bed while the nitrogen is adsorbed leaving oxygen as the primary component exiting in the product stream. Although this works quite well for oxygen recovery, it does not provide a means for nitrogen recovery.

[⊗] Abstract published in *Advance ACS Abstracts,* July 15, 1996.

(1) Haag, W. O.; Chen, N. Y. In *Catalyst Design: Progress and Perspectives*; Hegedus, L. S., Ed.; Wiley: New York, NY, 1987, pp. 163−212.

(2) Csicsery, S. M. In *Zeolite Chemistry and Catalysis*; ACS Monograph Series; American Chemical Society: Washington, DC, 1976; Vol. 171, p 680.

(3) Gates, B. C. *Catalytic Chemistry*; Wiley: New York, 1992.

(4) Ruthven, D. M. *Principles of Adsorption and Adsorption Processes*; Wiley: New York, 1984.

(5) Yang, R. T. *Gas Separation by Adsorption Processes*; Butterworth: Boston, 1987.

S0897-4756(96)00085-3 CCC: $12.00

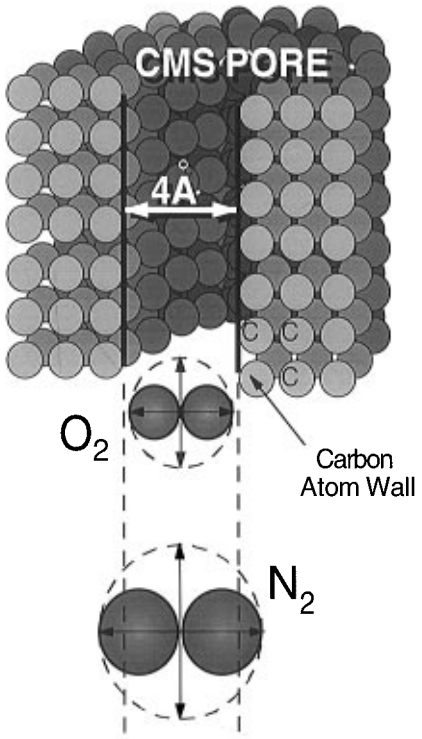

Figure 1. Schematic of oxygen and nitrogen approaching the nanopore of a CMS material.

In fact, nitrogen can be recovered from air by pressure swing adsorption (PSA), but it must be done over a very different kind of molecular sieve, and by a fundamentally different mechanism from oxygen recovery.[5] Rather than a crystalline aluminosilicate, a noncrystalline nanoporous carbon or carbogenic molecular sieve (CMS) is used. Instead of a separation produced by a difference in surface interaction potential at equilibrium, it is considered to be brought about by the difference in the rate of internal transport within the CMS, that is, by the kinetics of adsorption. The rates of approach to equilibrium for O_2 and N_2 in CMS are observed to be so substantially different while the equilibrium levels are quite similar, that it is concluded to be a separation based on size. This conclusion, derived empirically, was made even though the two adsorbates differ in kinetic radii by no more than 0.2 Å.[6] To illustrate this idea more clearly, the approach to the pore by O_2 and N_2 is shown schematically in Figure 1. Ironically, and somewhat paradoxically, the nanoporous carbon, with its ill-defined structure and nonsingular distribution of pore sizes, apparently produces a size-selective separation based only upon this difference of 0.4 Å in diameter. No zeolite, yet discovered, can duplicate this effect!

Evidence in support of the hypothesis that the separation is based upon size and, hence, kinetics has accumulated. Juntgen et al. were the first to demonstrate that separation could be conducted over a carefully prepared coal-derived CMS material.[7] It was their conclusion that a 4 Å sized pore was required to produce the requisite configurational barrier to nitrogen transport.[8] In later work Ruthven and co-workers compared air separation over zeolites with CMS and reported that the latter did indeed operate through a kinetic rather than an equilibrium-driven mechanism.[9] LaCava and the group at AIRCO-BOC also came to the same general result, concluding that kinetics of transport were the key to nitrogen recovery.[10] In contrast to Ruthven, who used a traditional linear driving force model to describe transport rates within the CMS, LaCava developed an analysis attributing the different transport rates of oxygen and nitrogen within the CMS to differences in the rate constants for Langmuirian adsorption and desorption. Despite the differences in their approaches to the analysis and modeling of the process, they obtained essentially the same results, and both agreed that *kinetics* were the underlying basis for the separation.

More recently, workers at Air Products and Chemicals have looked at this technology quite carefully.[11−13] Using a battery of new synthetic and characterization tools, including probe-molecule adsorption, they also conclude that the kinetics of sorption drive the separation. However, on the basis of the probe molecule studies, a slightly smaller pore size between 3 and 4 Å is considered to be optimal.[11] On the basis of these results and detailed modeling by Auvil et al., the Air Products Group was able to specify the best design and structure for a commercial CMS—a significant achievement and advance in nanoscale engineering design, especially considering how recently the primary separative effect was described.[12−14]

What is common to each of these studies is that they all relied upon the commercial PSA-type of CMS. This CMS is made by a method first described by Juntgen and co-workers at the Bergbau Forschung Institute for Coal Research.[5,7] A suitably prepared precursor, originally coal but more typically, now, a natural cellulosic material, such as coconut shells, is treated with a carbon deposition process in the final steps of its manufacture. A gas-phase precursor is cracked thermally over the precursor at a specific temperature and for a well-defined time in order to narrow the pores sufficiently to produce the molecular discrimination effect.

As useful and important as this process is for the commercial production of PSA-CMS, it is not readily adaptable to fundamental studies. First, and perhaps foremost, the details of the process are proprietary, and therefore, it is not easy to reproduce on a small scale. Both Suzuki et al. and Trimm et al. have published on the their attempts to simulate this type of deposition on a microscale in the laboratory.[15−17] Furthermore, the materials are difficult to prepare with systematic variations in their properties and characteristics, although Chihara and Suzuki eventually were successful.[17] For

(6) Suzuki, M. *Adsorption Engineering*; Elsevier: Amsterdam, Netherlands, 1990.
(7) Juntgen, H.; Knoblauch, K.; Harder, K. *Fuel* **1981**, *60*, 817.
(8) Juntgen, H. *Carbon* **1977**, *15*, 273.
(9) Ruthven, D. M.; Raghavan, N. S.; Hassan, M. M. *Chem. Eng. Sci.* **1986**, *41*, 1325.
(10) LaCava, A. I.; Koss, V. A.; Wickens, D. *Gas. Sep. Purif.* **1989**, *3*, 180.
(11) Moyer, J. D.; Gaffney, T. R.; Armor, J. N.; Coe, C. G. *Microporous Mater.* **1994**, *2*, 229.
(12) Braymer, T. A.; Coe, C. G.; Farris, T. S.; Gaffney, T. R.; Schork, J.; Armor, J. N. *Carbon* **1994**, *32*, 445.
(13) Cabrera, A. L.; Zehner, J. E.; Coe, C. G.; Gaffney, T. R.; Armor, J. N. *Carbon* **1993**, *31*, 969.
(14) Schork, J. M.; Srinivasan, R.; Auvil, S. R. *Ind. Eng. Chem. Res.* **1993**, *32*, 2226.
(15) Moore, S. V.; Trimm, D. L. *Carbon* **1977**, *15*, 177.
(16) Chihara, K,; Suzuki, M. *Carbon* **1979**, *17*, 339.
(17) Chihara, K.; Suzuki, M. *Bunri Gijutu* **1982**, *12*, 95 (in Japanese).

each of these reasons, no doubt, previous investigators (and would-be investigators) have shied away from serious attempts to define the fascinating interplay of nanostructure and surface chemistry that gives rise to this separation.

In light of these formidable problems, we have chosen to take a different tack to examine the transport of oxygen and nitrogen, that is, to study and compare polymer-derived CMS, prepared from poly(furfuryl alcohol), with commercial PSA-CMS.[18−20] In contrast to the commercial materials, these are prepared from high-purity and well-defined synthetic precursors. Furthermore, we have shown in previous work that their chemical and physical properties, especially porosity and pore size, may be varied in a systematic and controlled fashion by varying the temperature and time of thermal annealing.[19,21] Thus, the goal of this work was to compare the behavior of these PFA-CMS with commercial carbogenic sieves and to determine what effect, if any, the extent and duration of thermal annealing would have upon differential transport rates of nitrogen and oxygen. The separation of these two molecules, which are very close in size, was anticipated to be more demanding than any other molecules we had previously separated.[22,23] By examining the variations in the rates with changes in chemical and electronic properties, as well as physical pore sizes, we hoped to uncover what role these factors play in producing this remarkable separation of oxygen and nitrogen.

Experimental Section

CMS Preparation. The commercially available carbogenic materials that were studied, Takeda 5A and Airco PSA-CMS, were used as received without any further modification other than grinding. These commercial materials were chosen because the Airco PSA-CMS is a highly oxygen selective molecular sieve and the Takeda 5A is a completely nonselective material. As such, these materials demonstrate very different adsorption profiles for oxygen and nitrogen and essentially define the extreme boundaries of molecular discrimination within which the PFA-derived CMS will fall. Poly(furfuryl alcohol)-derived carbogenic molecular sieves were prepared by pyrolysis of PFA in an inert atmosphere according to previously established procedures.[7] The important steps in this process will be summarized here. Approximately 25 g of PFA was charged in a quartz boat, which was then placed inside a quartz tube reactor situated in a single-zone tube furnace. An inert atmosphere was established over the sample by flowing helium at 250 sccm through the reactor tube. The temperature of the sample was maintained by a ramp and soak temperature controller connected to a thermocouple suspended axially above the surface of the quartz boat. The furnace temperature was ramped at 10 °C/min from room temperature to 250 °C and held at this temperature for 2 h. The temperature was then raised at 10 °C/min to 400 °C and held for 2 h. Finally, the sample temperature was ramped again to the final maximum temperature of pyrolysis which varied from 400 to 1200 °C for each sample. This final pyrolysis temperature is defined as the synthesis temperature. The length of time the sample was held at this final temperature before cooling is referred to as the soak time and was varied from 0 to 8 h. The experimental CMS samples produced in this manner were crushed into smaller particle sizes for further testing.

O_2/N_2 Uptake Experiments. Oxygen and nitrogen uptakes were measured gravimetrically on a Cahn C-1100 high-pressure microbalance. This system consisted of a Cahn C-1000 microbalance contained in a stainless steel pressure vessel with stainless steel hang-down tubes on the sample and tare side of the balance. This unit has an ultimate sensitivity of 5 μg and can operate at pressures from 10^{-5} Torr to 1500 psi and temperatures up to 700 °C. The balance was fitted with a clam-shell furnace (Applied Test Systems, Inc., Model 3210) that surrounded the sample hangdown tube. Gas was introduced in an upflow fashion into the sample hangdown tube and the pressure was maintained using a Tescom back-pressure regulator.

All of the uptake measurements were made on samples of −60/+80 mesh particle size. Each sample was pretreated in the balance, prior to the uptake experiment, by heating in flowing helium (Keen Gas Co., 99.9%) to 120 °C until the mass of the sample reached a constant value. At this point the flow of helium was stopped, the sample allowed to cool to room temperature and a baseline weight was obtained. Then the balance was pressurized to 100 psia with the adsorbate to be studied, either nitrogen (Matheson, 99.99995%) or oxygen (Matheson, 99.997%). The adsorbate gases were dried over a bed of zeolite 5A to remove any residual moisture prior to introducing them into the balance. The initial shock wave caused by the rapid pressurization took on the order of 30 s to dissipate. Following this, weight measurements were made until equilibrium uptake was achieved (less than 0.01 mg/h weight change). Periodically a small quantity of adsorbate was introduced into the system to maintain the pressure at 100 ± 1 psia.

Data from the microbalance were collected on a strip chart recorder which was then scanned into the computer and converted to numerical columns of data. A buoyancy correction, based on the ideal gas law, was applied to these data. This correction amounted to about 1 mg and varied slightly depending on sample size. The buoyancy-corrected uptake data were then ratioed to the baseline sample weight to obtain intrinsic uptake vs time data which could be compared between samples.

Characterization. Photoacoustic infrared spectra were obtained with a MTEC Model 200 photoacoustic detector installed in a Nicolet 510M FTIR spectrometer. The optical bench was purged with moisture-free and CO_2-free air and the sample chamber of the photoacoustic detector was purged with high-purity helium (Keen Gas Co., 99.999%). Spectra were obtained for −60/+80 mesh particles that were evacuated at 10^{-3} Torr and 100 °C for at least 1 h before being placed in the spectrometer. A total of 500 coadded scans was collected for each sample, and the photoacoustic spectra were obtained from the ratio of the single-beam sample spectra to a graphite reference spectrum.

Mass magnetic susceptibilities of the PFA-CMS samples were measured using a Johnson Matthey MSB-Auto magnetic susceptibility balance with a magnetic field strength of 4.5 kG and an ultimate sensitivity of 5×10^{-10} cgs units. Measurements with this modified Guoy balance were made at room temperature and pressure on 100 mg samples of −60 mesh CMS particles.

Skeletal densities were measured using a Micromeritics Autopycnometer 1320 helium pycnometer. High-purity helium (99.999%) was supplied by Keen Gas Co. Prior to making the measurement, the samples were baked out at 120 °C in air for 1 h and then transferred while warm to the pycnometer and evacuated with a roughing pump for 10 min. This was done to remove residual moisture from the samples that could affect the accuracy of the density measurement.

High-resolution transmission electron micrographs of the PFA-CMS were produced using a Hitachi HF-2000 field emission transmission electron microscope (FE-TEM) located in the Materials Analysis User Center of the High Temperature Materials Laboratory at Oak Ridge National Laboratory.

(18) Lafyatis, D. S.; Tung, J.; Foley, H. C. *Ind. Eng. Chem. Res.* **1991**, *30*, 865.
(19) Mariwala, R. K.; Foley, H. C. *Ind. Eng. Chem. Res.* **1994**, *33*, 607.
(20) Foley, H. C. *Microporous Mater.* **1995**, *4*, 407.
(21) Foley, H. C.; Kane, M. S.; Goellner, J. F. In *Access in Nanoporous Materials*; Pinnavaia, T. J.; Thorpe, M., Eds.; Plenum: New York, 1995.
(22) Hong, A.; Mariwala, R. K.; Kane, M. S.; Foley, H. C. *Ind. Chem. Eng. Res.* **1995**, *34*, 992.
(23) Foley, H. C. *ACS Symp. Ser.* **1988**, *368*, 335.

This microscope has a point resolution of 2.3 Å and is equipped with a slow-scan CCD camera which allows for digital image collection, analysis, and processing. Samples were prepared for imaging by grinding the CMS in 2-propanol and dispersing a droplet of this solution onto a holey carbon film supported on copper grids.

The micrographs were acquired digitally using Digital Micrograph 2.5 software (Gatan Inc.) which allowed for further processing and analysis using NIH Image 1.57 and Image 1.28 image-processing software. The presence of organized structure in the micrographs was probed in more detail using fast Fourier transform (FFT) processing of the pixel data. This FFT analysis provides the digital equivalent of electron diffraction patterns and is interpreted in the same manner. Square regions of the micrographs were selected and a Gaussian mask was applied. This masking, evidenced by the white borders around the processed areas in the image, was done to minimize the appearance of cross-shaped features in the Fourier frequency domain (FFT) which are associated with sharp edge discontinuities caused by selecting a finite area for frequency analysis.[24] From this analysis, *d* spacings for organized features in small microdomains can be calculated from pixel spacings measured from the image.[25]

Neutron diffraction data were collected using the special environment powder diffractometer (SEPD) at the Intense Pulsed Neutron Source (IPNS) located at Argonne National Laboratory. The scattered intensity data were collected for 6 h (648 000 neutron pulses) and analyzed using the pair distribution function (PDF) technique.[26−28] The PDF analysis provides a real-space measure of the locations of near-neighbor atoms through Fourier transform analysis of the neutron diffraction data.

Results

Adsorption. *Equilibrium Adsorption of Oxygen and Nitrogen*. The uptakes of oxygen and nitrogen at 100 psia and 20 °C were measured on Airco PSA-CMS and Takeda 5A CMS (Figure 2). The results (Table 1) show that the equilibrium levels of adsorption of oxygen and nitrogen are within 10% on each CMS, with oxygen having a slightly higher equilibrium capacity in each case. The total uptakes for both materials are also very similar, on the order of 35−40 mg/g. Turning to the PFA-CMS samples, we note two trends (Figure 3). First, just as in the case of the commercial samples, the oxygen to nitrogen equilibrium adsorption ratios are similar, varying by no more than 20%, with the exception of the 400 °C sample which varies by approximately 40%. In every case oxygen is more strongly adsorbed than nitrogen. Second, the total uptake of both gases varies markedly with final pyrolysis temperature of the PFA-CMS. Uptakes are low for the 400 °C sample and rise dramatically with increasing pyrolysis temperature up to the 800 °C material, which has a total uptake quite close to the commercial control samples. For the CMS synthesized at 1000 and 1200 °C the uptakes of oxygen and nitrogen are essentially zero (Figure 4). The total pore volume accessible to oxygen and nitrogen therefore goes through a maximum which occurs with the 800 °C material.

Rates of Transport and Adsorption. The rates of approach to adsorptive equilibrium were measured for the two control samples, commercial PSA-CMS and Takeda 5A, and the six PFA-CMS samples (Figures 2 and 3). Comparing the two control samples first, we note that the characteristic of the commercial PSA-CMS is the extraordinarily rapid rise in oxygen uptake as a function of time versus the much slower approach to equilibrium displayed by nitrogen. It is quite noticeable that the slopes of these curves are distinctly different. In contrast, for the Takeda 5A CMS, which is known not to produce the requisite molecular sieving effect, the character of the two uptake curves is quite similar and both gases attain their respective equilibrium adsorption levels at similar rates. This behavior is expected: the pores in the Takeda 5A are too large to provide the molecular discrimination between oxygen and nitrogen, whereas the commercial PSA-CMS is very effective at separating these gases. These very different adsorption profiles define the extremes of selectivity within which the PFA-derived CMS fall.

Adsorptive uptake curves for nitrogen and oxygen under the same conditions are displayed for the 400, 600, 700, and 800 °C PFA-CMS samples (Figure 3). It is clear that for each sample the rate of oxygen adsorption is much faster than the rate of nitrogen adsorption.

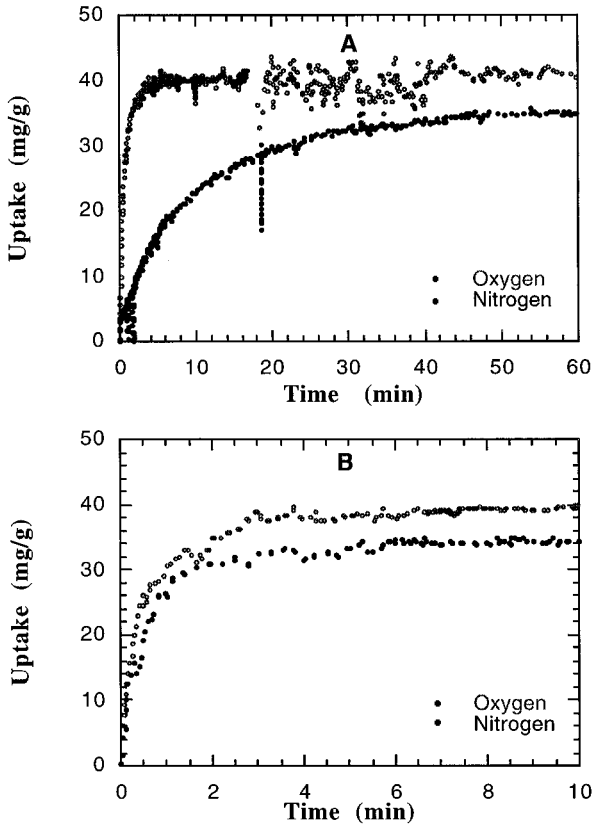

Figure 2. Oxygen (○) and nitrogen (●) mass uptakes as a function of time on commercial Airco PSA-CMS and on Takeda 5A CMS (P = 100 psia, T = 25 °C).

Table 1. Equilibrium Adsorption Capacity of Oxygen and Nitrogen on Commercial CMS Samples at 100 psia and 25 °C

	equilibrium capacity (mg/g)	
adsorbate	Takeda MSC 5A (nonsieving)	Airco PSA-CMS (sieving)
oxygen	40.5	40
nitrogen	36.5	36.7
ratio of oxygen-to-nitrogen equilibrium adsorption	1.11	1.09

(24) Reeves, A. FFT Extension to Image 1.25, Public Domain Software Documentation, Dartmouth College, 1990.
(25) Cao, S.; Allard, L. F. Lattice Fringe Space Measurement Using Fourier Transform in Digitized HRTEM Image, to be submitted, 1995.
(26) Egami, T. *Mater. Trans.* **1990**, *31*, 163.
(27) Warren, B. E. *X-ray Diffraction*; Addison-Wesley: Reading, PA, 1969.
(28) Klug, H. P.; Alexander, L. E. *X-ray Diffraction Procedures for Polycrystalline and Amorphous Materials*; Wiley: New York, 1992.

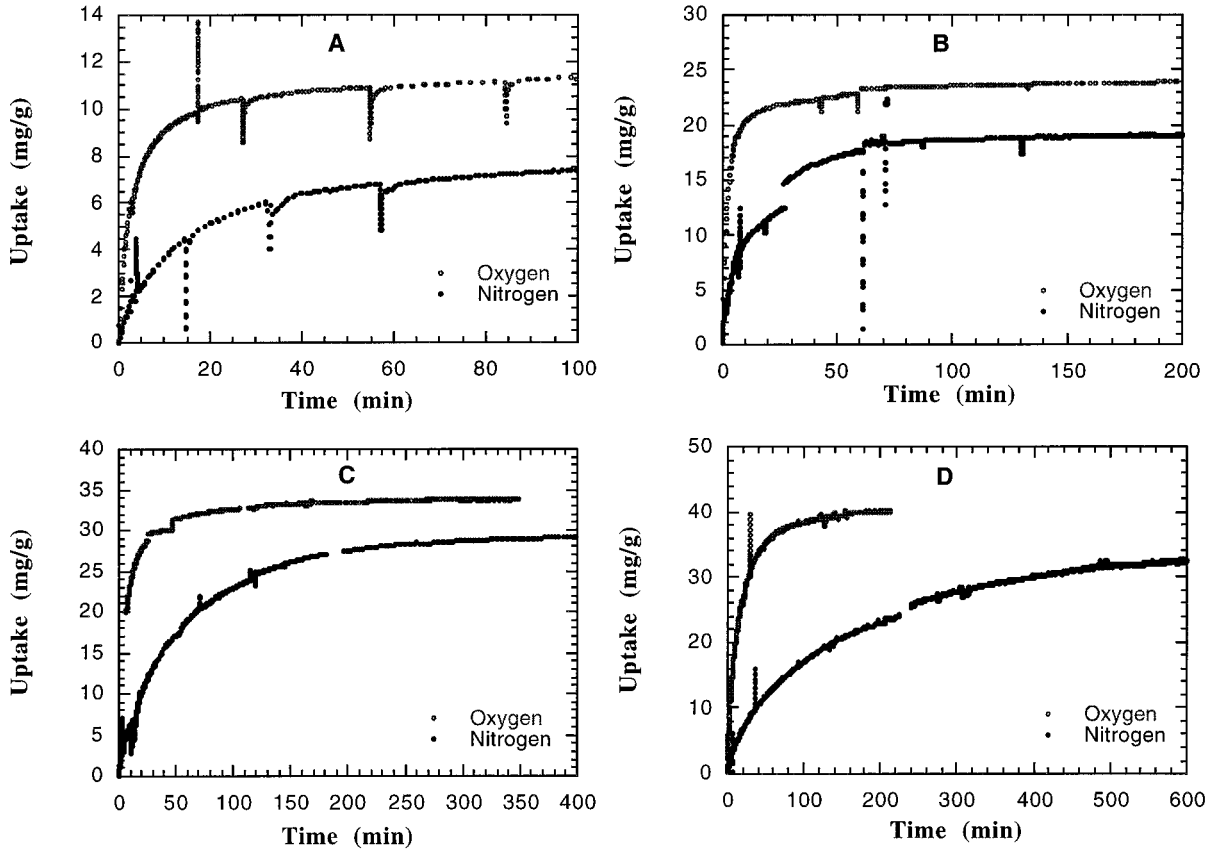

Figure 3. Oxygen (○) and nitrogen (●) mass uptakes as a function of time on 400, 600, 700, and 800 °C PFA-CMS (P = 100 psia, T = 25 °C).

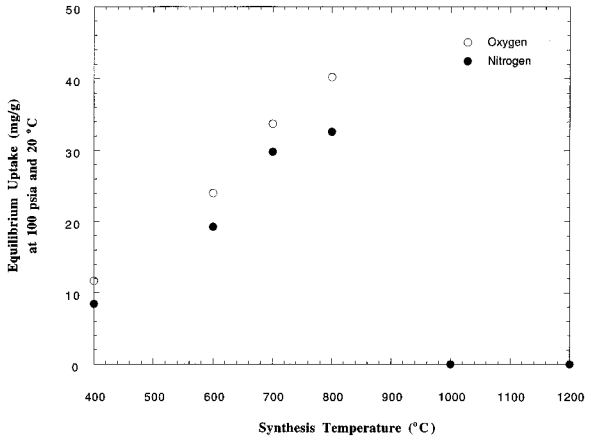

Figure 4. Equilibrium capacities for oxygen and nitrogen as a function of synthesis temperature for PFA-CMS.

Also, it is notable that the extent of oxygen adsorption is higher than that of nitrogen, as was mentioned earlier.

From these time-dependent data, we can calculate diffusivities for oxygen and nitrogen that can be compared to those of carbon dioxide which were measured previously. These effective diffusivities, D_e, are obtained by fitting the mass uptake versus time data to the following expression:

$$\frac{M}{M_\infty} = 1 - \frac{6}{\pi^2}\sum_{n=1}^{\infty}\left[\frac{1}{n^2}\exp\left[-n^2\pi^2 D_e\frac{t}{r^2}\right]\right]$$

The infinite series was truncated after 20 terms, and since the diffusivities are used only for the purpose of structural comparison, no attempt was made to correct for concentration dependence. The data determined in this fashion for the PFA-CMS samples are collected in Table 2. We know that all the diffusivities, including those measured previously for carbon dioxide, are in the range 10^{-9}–10^{-8} cm^2/s. This clearly is within the so-called "configurational" diffusion regime. The same measurements made for Takeda 5A CMS resulted in diffusivities on the order of 10^{-7} cm^2/s. In contrast the commercial PSA CMS displayed diffusivities of 10^{-7}–10^{-9} cm^2/s (Table 3).

The diffusivities of oxygen and nitrogen are plotted in Figure 5 as a function of temperature of preparation. Also, on the plot are the diffusivities measured earlier

Table 2. Effective Diffusivities for Nitrogen, Oxygen, and Carbon Dioxide in PFA-CMS (Carbon Dioxide Data[19])

final pyrolysis temp (°C) (8 h soak)	adsorbate effective diffusivity (cm^2/s)		
	nitrogen	oxygen	carbon dioxide
400	2.43×10^{-9}	1.86×10^{-8}	
500			5.1×10^{-9}
600	3.08×10^{-9}	3.13×10^{-8}	6.3×10^{-8}
700	1.60×10^{-9}	1.08×10^{-8}	
800	8.39×10^{-10}	6.02×10^{-9}	3.1×10^{-8}
1000			8.0×10^{-10}

Table 3. Effective Diffusivities of Oxygen and Nitrogen in Commercial CMS Samples

adsorbate gas	effective diffusivity (cm^2/s)	
	Takeda MSC 5A (nonsieving)	Airco PSA carbon (sieving)
oxygen	1.25×10^{-7}	1.65×10^{-7}
nitrogen	1.14×10^{-7}	8.50×10^{-9}
ratio of oxygen-to-nitrogen effective diffusivities	1.10	19.41

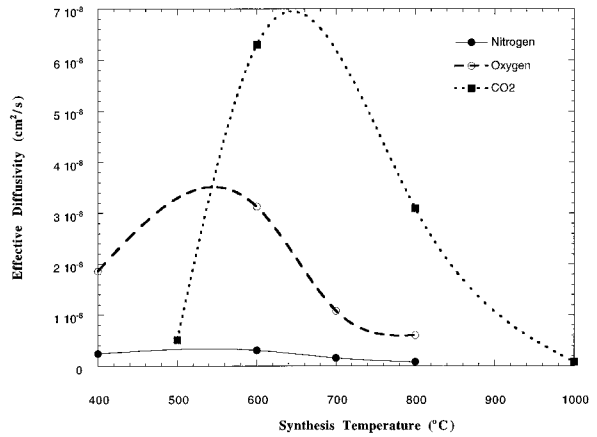

Figure 5. Effective diffusivities for oxygen and nitrogen versus the final annealing temperature of the PFA-CMS materials.

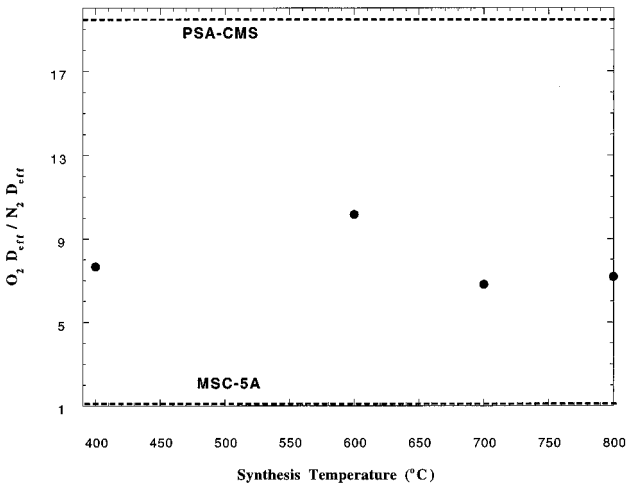

Figure 6. Ratios of oxygen to nitrogen effective diffusivities over 400, 600, 700, and 800 °C PFA-CMS, commercial PSA-CMS, and Takeda 5A CMS.

for carbon dioxide. Although the carbon dioxide measurements were done at lower pressure (760 Torr) versus 100 psia for the nitrogen and oxygen, we note that both the oxygen and carbon dioxide effective diffusivities show a distinct maximum in the vicinity of the 600 °C annealing temperature. The nitrogen diffusivity is lower in all cases and appears essentially constant over the same range of temperatures, but its diffusivity also maximizes with the 600 °C sample.

Finally, the oxygen and nitrogen diffusivities may be ratioed in order to evaluate a theoretical separation factor. This has been done, and the results are accumulated in Figure 6. The separation factor calculated in this way for the Airco PSA-CMS is higher than 19 and at the other end of the spectrum the Takeda 5A carbon falls to 1. Intermediate between these are the values for the PFA-CMS samples which fall in the vicinity of 6−10. The variation between the value for each of the samples is small with the ratio maximizing for the 600 °C sample at a value of 10.2.

Characterization. To understand the results of oxygen and nitrogen adsorption on the PFA-CMS materials, we set out to extend the physical, chemical, and morphological characterization data that we already had from previous work. New data were sought that could be useful in providing some deeper understanding of the adsorptive selectivity in this particular case.

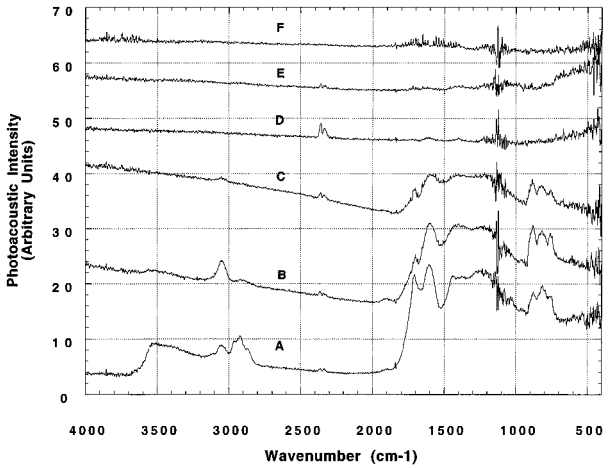

Figure 7. Photoacoustic spectra (PAS) of the PFA-CMS materials: (A) 400, (B) 500, (C) 600, (D) 700, (E) 800, and (F) 1000 °C.

Photoacoustic Spectroscopy. The functional groups in poly(furfuryl alcohol) include the heteroatom oxygen of the ring as well as residual hydroxyl groups terminating chains. Fitzer and Schaeffer reported that upon heating PFA, carbon monoxide or formaldehyde insertion leads to carbonyl bridges in the structure of the partially pyrolyzed polymer.[29] Photoacoustic spectra for the PFA-CMS are displayed in Figure 7. It is clear that the 400 °C PFA-CMS sample is rich in hydroxyl groups, as evidenced by the broad band between 3100 and 3500 cm^{-1}, and in carbonyl groups, indicated by the intense band at 1710 cm^{-1}. From previous work, we also know that this material is fairly hydrogen-rich with a H/C atom ratio of 0.5. It is clear that some of this hydrogen is attached to aromatic ring carbons since there is an aromatic carbon−hydrogen stretch at 3100 cm^{-1} and the out-of-plane bending modes for the same hydrogens are prominently displayed in the three bands centered at 800 cm^{-1}. Interestingly, the bands around 2900 cm^{-1} indicate that some hydrogen is present in aliphatic form. In addition to those spectral features which can be attributed to remnants of the PFA precursor, the broad band between 1000 and 1700 cm^{-1} is indicative of the infrared absorption by the carbon-carbon backbone of the developing CMS structure.

Having assigned the primary features of the lowest temperature material, we can now examine the effect of thermal annealing on the evolution of the functional groups and, concomitantly, upon the spectra of the materials that result. Comparing the 500 °C sample's spectrum to that of the 400 °C material's spectrum, we find notable changes (Figure 6b). The hydroxyl band has dropped to an insignificant level of intensity and so too have the bands due to C═O bonds at 1710 cm^{-1}. At the same time the aromatic C−H band's intensity has grown, as have the bands attributed to their out-of-plane bending modes. Consistent with these observations is the noticeable drop in the intensity of the band arising from the stretching of the aliphatic C−H bond.

With the 600 °C (Figure 6c) sample we note that the bands due to the aromatic C-H stretching, the out-of-plane bends and the bands attributed to C═O bonds, all drop significantly in intensity. This indicates that

(29) Fitzer, E.; Schaeffer, W. *Carbon* **1970**, *8*, 353.

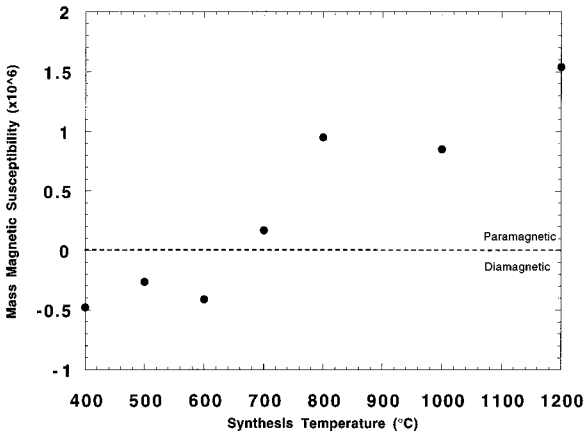

Figure 8. Effect of final annealing temperature on mass magnetic susceptibility of PFA-CMS materials.

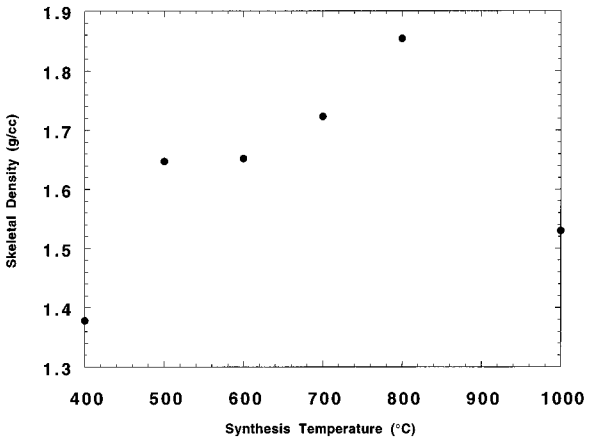

Figure 9. Variation in skeletal densities of PFA-CMS with increasing annealing temperature.

most of the oxygen heteroatoms and a significant fraction of the hydrogen have left the solid, both interpretations are supported by previous chemical analysis and ^{13}C MAS-SS NMR results on these samples.[19] As the synthesis temperature is raised even further, the spectra become essentially featureless (Figure 6d−f). All of the photoacoustic spectra are obtained by ratioing the single-beam sample spectra to a graphite standard spectrum. The flat photoacoustic spectra indicates that the sample single-beam spectrum is identical with that of graphite. This can be attributed to the loss of heteroatoms and hydrogen in the solid. As the sample becomes more aromatic and chemically similar to graphite, it more strongly absorbs infrared energy. In the limit of this process, the sample spectrum, like that of graphite, is essentially a measure of the power spectrum of the spectrometer, so the resulting photoacoustic spectrum is flat and featureless. Once again, these results and interpretations are corroborated by chemical analysis and solid-state nuclear magnetic resonance spectroscopy.[19]

Magnetic Susceptibility. Since heteroatoms and hydrogen are ejected from the solid structure upon heating at elevated temperatures, it is logical to ask how the electronic structure of the material changes. Magnetic susceptibility measurements provide a sensitive measure of the free electron density in the material. Presumably, these unpaired electrons are vestiges of bonds broken during pyrolysis and are best thought of as dangling bonds. Thus, as a sample becomes richer in unpaired electrons, its magnetic susceptibility increases and, eventually, it becomes net paramagnetic.

The evolution in magnetic properties of samples with thermal annealing at progressively higher temperatures is tracked by the changes in their magnetic susceptibilities (Figure 8). The three PFA-CMS samples prepared below 700 °C are diamagnetic with mass susceptibilities, X_g, between -5×10^{-7} cm^3/g and zero. With the 700 °C sample, the mass magnetic susceptibility crosses over to positive values in the paramagnetic region. The samples prepared at 1000 and 1200 °C have an even higher degree of paramagnetism, maximizing at 1.5×10^{-6} cm^3/g for the 1200 °C sample.

Helium Pycnometry. The primary interest in these materials lies in their molecular sieving properties. Thus examining changes in their physical structure, along with their chemical transformations, is paramount. Helium pycnometry is useful for this because it provides a direct measure of the solid's skeletal density and since helium is inert and quite small (2.55 Å), it is not adsorbed appreciably at 25 °C and it typically finds access through very narrow pores.

The skeletal densities of the PFA-CMS samples prepared between 400 and 800 °C vary from a low of 1.38−1.85 g/cm^3 as shown in Figure 9. Thus, an increase in density accompanies the increase in final pyrolysis temperature to this point. However, at 1000 °C the skeletal density apparently drops to 1.5 g/cm^3.

High-Resolution Transmission Electron Microscopy. Along with the chemical changes that follow from high-temperature thermal annealing, it is important to examine morphological and textural changes especially in the nanostructures of the solids. For these purposes four samples were selected for examination, the 400, 500, 800, and 1200 °C samples of PFA-CMS.

Examination of the HRTEM images reveals a clear progression in nanostructure (Figure 10a−d). The 400 and 500 °C samples show little or no structure even on the nanometer or shorter length scale. An FFT analysis of the selected region in the micrograph for the 400 °C CMS (Figure 11) provides further evidence that the structure is underdeveloped. The presence and number of spots in the FFT, which is essentially a diffraction pattern, indicate the degree of ordering in the structure. There are two spots in the FFT, from which a *d* spacing of 2.03 Å can be calculated. This spacing is in good agreement with the 2.03 Å spacing associated with the (101) plane of graphite. The (101) plane and its *d* spacing are related to the in-plane carbon−carbon bond distances in the aromatic structure of graphite. Conspicuous in their absence are any diffraction spots characteristic of the 3.36 Å *d* spacing characteristic of the (002) plane of graphite. This is the familiar interlayer distance between the infinite sheets of hexagonal carbon atom arrays in graphite. These results show that at this low temperature the carbon atoms are beginning to organize themselves into aromatic domains, but these aromatic nanodomains have not organized into the three-dimension layered structure like that found in graphite.

With the higher temperature material, we observe the onset of distinct microstructure at 800 °C. The layers of carbon that are evident are parallel, but the overall domain sizes remain relatively small. Furthermore, the number of parallel layers in one domain is relatively small, only three to five in number and not enough to

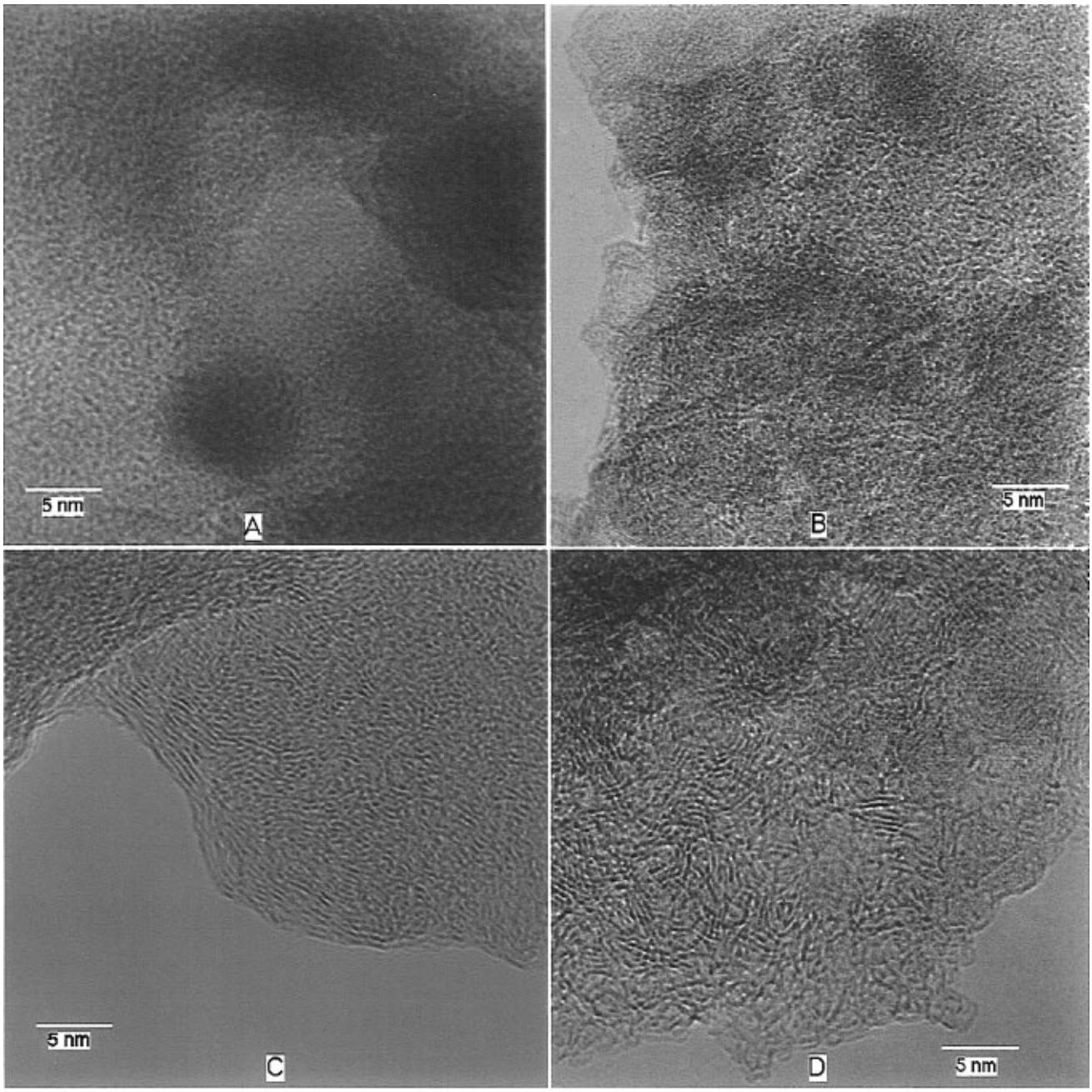

Figure 10. High-resolution transmission electron (HRTEM) microscopy images of PFA-CMS: (a) 400, (b) 500, (c) 800, and (d) 1200 °C.

diffract as graphite. In the 1200 °C sample, the structure has developed to longer length scales. The nature of the nanostructural reorganization occurring at this higher temperature is probed using FFT analysis of a micrograph for the 1200°C CMS (Figure 12). In this micrograph we can see that the aromatic microdomains which were beginning to form at low temperatures have now organized into more well-defined layered structures. An FFT analysis of the selected region in Figure 12 indicates that the spacing between the layers visible in the micrograph is 3.41 Å. This is very close to the 3.36 Å interlayer spacing in graphite. At this higher temperature the nanodomains are organized into layered structures that begin to take on the three-dimensional structure of graphite, but only on very small length scales. We also notice that the parallel carbon layers remain, for the most part, parallel, but with the growth of these domains comes the onset of local curvature. The ultimate example of this is a feature in this material that is a set of imperfect concentric rings. The curvature increases as a function of position; near the center of this feature radii of curvature approach 4 Å. At the innermost portion of the feature, where the radius of curvature would fall below 4 Å, the image becomes indistinct and structurally ill-defined.

Discussion

The adsorption results indicate the extent to which the rate of transport of oxygen exceeds that of nitrogen in the selective CMS materials. Comparison of results with Takeda 5A CMS, a material that is not selective toward oxygen, opposed to the Airco PSA-CMS used commercially, make this plain. The PFA-CMS materials are selective to oxygen as the data show. Yet, it is

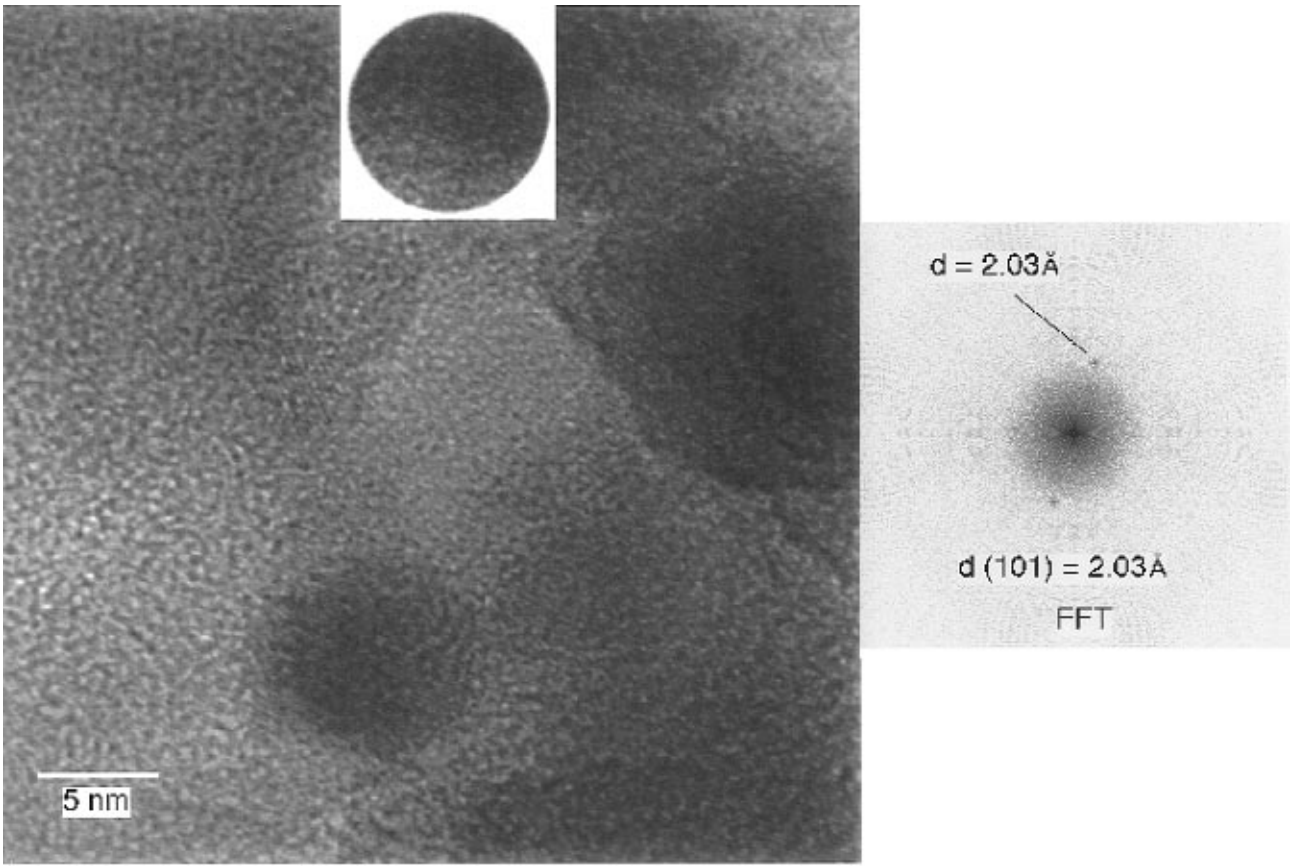

Figure 11. High-resolution electron micrograph of PFA-CMS synthesized at 400 °C with FFT of selected region.

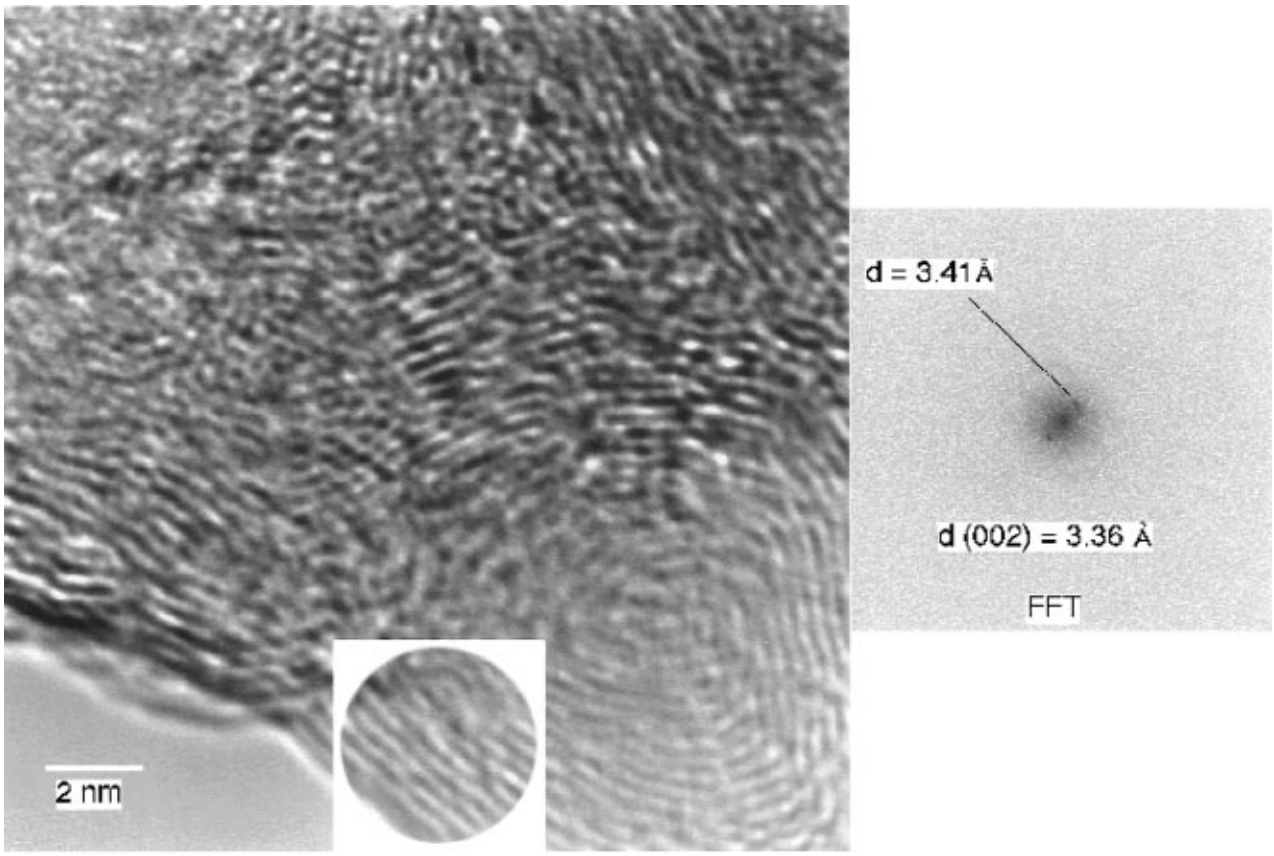

Figure 12. High-resolution electron micrograph of PFA-CMS synthesized at 1200 °C with FFT of selected region. The highly curved region of carbon in the lower right corner is reminiscent of the "onionskin" fullerenes.[31−35]

also worth noting that all the carbons examined show a preference for oxygen over nitrogen at equilibrium, and this is independent of the rate of approach to that equilibrium.

The separation factors for the PFA-CMS materials are roughly half those measured for the Airco PSA-CMS. This arises from somewhat lower oxygen diffusivities in the PFA-CMS materials and similar nitrogen diffusivities. The results suggest that the pore sizes of the PFA-CMS materials may be smaller on average than those in the Airco PFA-CMS. Partial support for this hypothesis comes from the fact that the overall rates of adsorption, that is the time to reach equilibrium is much slower for the PFA-CMS. We must be cautious not to extend this interpretation too far, since implicit in the analysis, and thus the valuation of the diffusivity, is the assumption that interfacial areas are the same. [Although the particle sizes are the same, and the interfacial area is the same it is not clear that the number of pore openings and their total areas are equal. More specifically it is assumed that the area of the pore faces through which the flux transports is the same. This may not be a good assumption, since it has not been confirmed, but to do so is a separate and challenging problem.] Thus, any changes in the area available for flux transport with final annealing temperature may actually be mathematically lumped into the effective diffusivities.

Looking more closely at the equilibrium levels of adsorption, it is notable that the 400 °C PFA-CMS sample has a low, but finite, level of uptake for both oxygen and nitrogen. This structure also has the lowest magnetic susceptibility and the most chemical structure, a point made clear by its photoacoustic spectrum. Between 400 and 800 °C there is an almost linear increase in the adsorption of oxygen and nitrogen. In the same regime the magnetic susceptibility grows and the materials become distinctly paramagnetic. Consistent with these changes are those that take place in the photoacoustic spectra. These observations indicate that as the heteroatoms exit the structure, they leave behind stable free radicals and at the same time generate considerable porosity in the solid. What happens next is most interesting. The apparent or accessible porosity of the solid drops to essentially zero between 800 and 1000 °C, so that the samples prepared at 1000 and 1200 °C *do not adsorb* oxygen and nitrogen.

It is interesting to compare results obtained with oxygen and nitrogen at 100 psia and 25 °C with those obtained with carbon dioxide at 15 psia and 25 °C. As we have shown in earlier work, the total uptake of CO_2 is low in the 400 °C sample (<10 mg/g), rises slightly in a 500 °C sample (10 mg/g), increases drastically to over 90 mg/g with the 800 °C PFA-CMS, and then falls to near zero levels with 1000 °C treatment and beyond. These results with O_2, N_2, and CO_2 correlate remarkably well. Both sets of experiments indicate that the structure of the solid moves along a sequence from underdevelopment, to full development and accessibility, to a stage of overdevelopment with respect to total adsorption and accessible free volume. The maximum accessible porosity in PFA-CMS occurs between 600 and 800 °C. Effective diffusivity measurements on the same samples with carbon dioxide show a maximum with the 600 °C sample, and then the values fall nearly linearly between the 600 and 1000 °C preparation temperatures. Hence, the overall range of diffusivities can be varied by approximately 2 orders of magnitude simply by adjustment of the thermal annealing temperature. It seems significant that the diffusivity for oxygen also maximizes near the 600 °C annealing temperature; however, the range of diffusivities varies in this case by just one order of magnitude. Nitrogen shows a slight maximum in diffusivity in the vicinity of the 600 °C sample, but the dynamic range of diffusivities for nitrogen over this range of annealing temperature is somewhat smaller.

Although the adsorption results indicate a maximization of available void volume in the sample, the skeletal density of the samples rises nearly linearly with annealing temperature to 800 °C. The lowest density material, the 400 °C PFA-CMS, displays a low total uptake for O_2, N_2, and CO_2. Initially, this seems contradictory, since one might have expected the lowest density solid to have the most void volume. However, if one returns to the photoacoustic spectrum, we note that this sample's spectrum is truly rich with functional groups. Furthermore, the sample is the most diamagnetic of the set. Its low density is not due to available void volume but rather to a structure that is intermediate between the initial polymer and the high carbon solid. Although a polymer would be able to *absorb* and, hence, dissolve some volume of gas, this sample is too rigid to rearrange and solvate the intruding gases. As a result, both *adsorption* and *absorption* on the 400 °C sample, are limited, physically, to low levels.

Examination of the HRTEM image of the sample prepared at 400 °C reveals a very homogeneous and structurally isotropic solid. The lack of structure indicates that there is relatively little in the way of void volume for adsorption, as was inferred from the arguments of the previous paragraph. The structure also is one that is highly symmetric, so symmetric that it approximates or tends toward the symmetry of a plane. Systems of such high symmetry are inherently unstable,[30−32] since if symmetry can break it will. In other words, if there is a pathway by which this highly symmetric form and morphology can evolve to a more stable structure, then the transformation is favorable and likely. The pathway in this system is the elimination of heteroatoms first, followed by loss of dihydrogen and, eventually, by the collapse of free volume with the diminution of surface area.

Turning to the samples prepared between 400 and 800 °C, we have noted that the functional groups drop in intensity drastically. From previous work the H/C ratio decreases sharply, and the void volume grows to a maximum. At the same time, the skeletal density grows as does the magnetic susceptibility. Clearly, the changes in the chemical and accompanying physical properties are high energy, that is, highly activated transformations. This high-energy requirement can account for the formation of paramagnetic, or free radical, sites being left behind in the solid as the heteroatoms and dihydrogen are released. Free radicals of the type shown below have been synthesized in molecular form, are indefinitely air stable, and are,

(30) Stewart, J.; Golubitsky, M. *Fearful Symmetry*; Penguin: London, UK, 1992.

(31) Kane, M. S.; Goellner, J. F.; Foley, H. C.; Billinge, S. J.; Allard, L. F. *Science*, submitted.

(32) Anderson, P. W. *Basic Notions of Condensed Matter Physics*; Benjamin-Cummings: Menlo Park, CA, 1984; pp 262−286.

perhaps, good models for the types of kinetically stabilized radicals entrapped in the solid.[33] The HRTEM

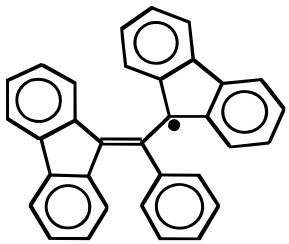

results show that with temperature the structure moves from the highly symmetric, disordered solid of 400 °C to one that is less symmetric, less disordered, and locally highly structured at 800 °C. On the short length scale of the aromatic or graphene-like domains we note parallel, straight walls. Between these domains is less well-developed material. The material appears to be a mixture of symmetric, or "ordered" carbon, and unsymmetric, or "disordered" carbon. The orientation of the locally ordered domains is random; no preferred direction appears. However, the overall symmetry of the structure has dropped and the isotropy of the low-temperature structure is lost. The morphological symmetry of the low-temperature solid has been broken.

At this point we are faced with a seeming contradiction—the gas adsorptivity has risen sharply as the skeletal density has increased. The explanation lies in the combination of the photoacoustic spectra and magnetic susceptibility measurements with the micrographs. The 800 °C PFA-CMS shows a lowered morphological symmetry, a sharp rise in paramagnetic susceptibility, and the loss of hydrogen and vestigial functional groups. But, the material is a mixture of more-dense graphene-like material and less-dense carbon in trigonal, sp^2, geometry (based upon ^{13}C SS-MAS NMR[19]). The free volume for gas adsorption is created within the void spaces formed between the subgraphitic domains. The disclinations and misalignments between these domains maximize at 800 °C and create, therefore, the largest available porosity. Thus, the process of symmetry breaking in the solid is intimately involved in the formation of the molecular sieving structure of the carbon. If symmetry breaking is the cause, then nanopores are its direct, physical effect.

Above the 800 °C treatment temperature, adsorption falls sharply in the PFA-CMS materials. This drop is observed with all the gases we have tested to date, not just with nitrogen and oxygen. The cause of this effect could be either closure of the pore mouths with temperature or total densification leading to both pore mouth narrowing and internal volume shrinkage. If this were brought on solely by pore entrance narrowing or blockage, then the free volume would be retained but rendered inaccessible. In other words, the internal porosity would not be destroyed or diminished but, simply, would be rendered unavailable. On this basis then, the skeletal density should be expected to be fairly low compared to graphite and not too different from that of the 800 °C sample. On the other hand, if the pore mouths contract and the internal free volume collapses with them, then the density would continue to increase with higher temperature and would approach that of graphite. Surprisingly, we find the skeletal densities of the 1000 and 1200 °C both to be about 1.5 mg/g, a value well below the 2.25 mg/g expected for graphite. This strongly suggests that pore mouth narrowing or closure occurs, with temperature, and it occurs without a significant loss of the internal void volume of material. In other words, if even helium is unable to penetrate the narrowed pores (despite its small kinetic diameter of 2.333 Å), then the apparent volume of the material appears to be high, but due to the presence of inaccessible internal voidage, its mass is low. These two effects in combination produce a density that is artificially lowered. Simply put, a density of 1.5 mg/g is an artifact of the experimental method.

The pore entrance narrowing process is brought on by further ordering of the material. Returning to the notion of this material as a solid mixture of ordered graphene-like domains and relatively homogeneous, but disordered carbon, the higher annealing temperatures lead to a steady conversion of the disordered carbon into locally ordered carbon. Presumably, the most active and mobile form of the carbon in the structure is at the pore mouths. Thus, we would expect the subgraphitic domains to grow in size and to decrease in number at their expense. Both expectations are met. Examination of the HRTEM image of the 1200 °C PFA-CMS indicates considerable elongation of the subgraphitic domains and significant local ordering in the sample. However, there is an unanticipated result. Rather than converting into true graphitic nanodomains embedded in the solid, we find that the nanodomains of the 1200 °C material have grown into snakelike structures with regions of very high local curvature. As a result, these domains occupy more space in the solid than do well-oriented nanocrystals. Although there is curvature, the layers of carbon atoms remain parallel. This curvature serves to break the local symmetry that would lead to elongated, straight domains of actual nanoscale graphite. Furthermore, because of this the number of layers in parallel remains rather low in number, usually well below 10. It is no surprise then that X-ray diffraction in this sample results only in broad, low-intensity patterns, located in the vicinity of those lines attributable to graphite, and just as intense as these broad peaks is a peak at a 2θ value corresponding to $\sim$5 Å (17°) which has been attributed to the so-called "turbostratic" structure of carbon.[19] It is noteworthy that despite the rather significant rearrangements that have occurred in nanostructure, the X-ray diffraction patterns of each of these materials appear more similar to each other than they do to graphite.

Pursuant to uncovering of the local nanostructure are neutron diffraction results for the 1200 °C PFA-CMS. Neutron diffraction data were collected in the form of the total structure function $S(Q)$, where Q is the momentum transfer of scattered neutrons. Fourier transformation of the structure function converts the data into the real-space atomic pair distribution function (PDF). The PDF provides the atomic structure of nonperiodic materials, like CMS, through a real-space measure of the locations of near-neighbor atoms. The presence of peaks in the PDF correspond to distances between correlated pairs of atoms. Comparison of the pair distribution function (PDF) of the specimen with a

(33) Koelsch, C. F. *J. Am. Chem. Soc.* **1957**, *79*, 4439.

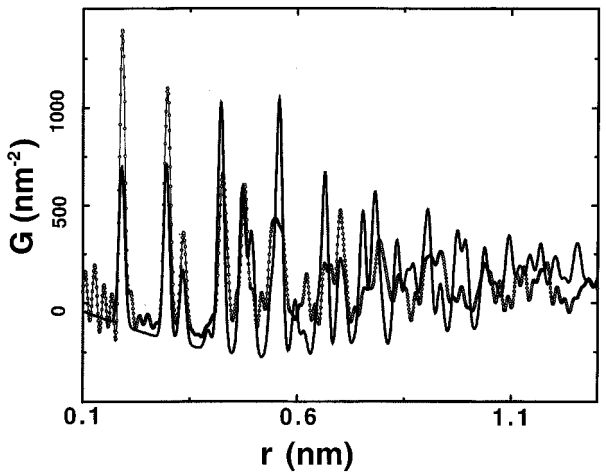

Figure 13. Comparison of PDF for 1200 °C sample (○—○) with calculated PDF based on crystal structure of graphite (—).

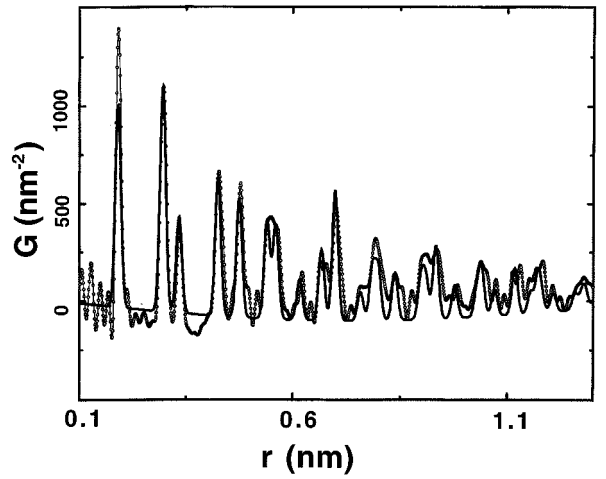

Figure 14. Comparison of PDF for 1200 °C sample (○—○) with calculated PDF based on structure of single graphene sheet (—).

calculated PDF based on the crystal structure of graphite is instructive. We find that the fit between these two is rather poor at all distances beyond 4−5 Å (Figure 13). Instead of graphite, if we compare to a calculated PDF for a single layer of graphite, that is, to a single two-dimensional *graphene* sheet, then the agreement increases substantially (Figure 14). This is consistent with the subgraphitic nature of this solid. Further, the agreement indicates that the correlated, or coherent, nanostructure extends to no more than 15 Å and then falls off. This indicates local domains with 30 Å coherence lengths, a value in good agreement with the HRTEM images and with earlier work we have done using a combination of xenon adsorption and ^{129}Xe NMR spectroscopy.[34]

One of the significant findings of this work has been the observation with HRTEM of domains consisting of evenly spaced, imperfect concentric rings of carbon layers. One such layered structure is displayed in Figure 12. As the structure is traversed in the radial direction toward its center, the degree of curvature increases. The radius of curvature of the outer rings is approximately 20 Å, but this falls to about 4 Å toward the inner boundary of the structure. It is also noteworthy that there is considerable structural dissonance at the center of this structure displayed in the image. This is not an aberration but instead a real morphological property of the structure. Below a value of 4 Å in radius of curvature it is entirely logical to expect coherent carbon structures to end, since the structure and bonding of sp^2 type carbon precludes any smaller radii of curvature without excessive strain energy.

(34) Bansal, N.; Foley, H. C.; Lafyatis, D. S.; Dybowski, C. *Catal. Today* **1992**, *14*, 305.

Conclusions

We have found that the PFA-CMS will distinguish between oxygen and nitrogen on the basis of their kinetics of adsorption. This is the first comprehensive study of PFA-derived CMS to explore the link between the high-temperature physical and chemical microstructural reorganizations in these polymer-derived materials and their molecular sieving character. Although each of the materials examined, including the commercial materials, adsorbed more oxygen than nitrogen at equilibrium, the difference is not significant enough to lead to useful separations. The data accumulated here point to a purely kinetic-based separative mechanism in agreement with the hypotheses of earlier workers. There is no correlation between the kinetics of separation and the magnetic susceptibility of the materials. However, the magnetic susceptibility measurements do provide a measure of increasing structure development, as does the photoacoustic infrared spectra. At the intermediate state of 800 °C pyrolysis temperature, the sample is paramagnetic and open, displaying the highest oxygen loading at equilibrium. Thus, the oxygen capacity may be thought to rise with magnetic susceptibility, but even this is complicated by other effects. The 1000 and 1200 °C samples are even more paramagnetic than the 800 °C sample, but their pores are too narrow for oxygen to diffuse in, so the measured capacity is zero despite large values of paramagnetism.

High resolution electron micrographs offer the first clear-cut analysis of nanostructure and morphology in these CMS materials. The maximum separation factor occurs in the 600 °C PFA-CMS, which is a mixture of both locally ordered and globally disordered carbon at the nanoscale. This mixture provides the best, or optimal, oxygen transport result. Samples prepared above 1000 °C continue to evolve structurally, as indicated by the growth in their paramagnetism and the complete loss of photoacoustic signal. However, these materials do not provide accessible void volume, not even to helium, and are not useful as molecular sieves. On the basis of HRTEM, the reason for this is that a highly developed snake- or ribbonlike nanostructure takes form in these materials. It is this characteristic of more extended short-range order on a length scale of 30 Å that is associated with near-zero levels of adsorption for oxygen, nitrogen, and carbon dioxide. Skeletal density measurements indicate that rather than having undergone a total densification with temperature, these materials have undergone pore entrance closure (or near closure) with retention of internal free volume. Since helium cannot access the free volume, the pore mouths are probably less than 2.3 Å in size, or for all intent and purposes closed, since below this value the pore size begins to approach the carbon-to-carbon bonding distance. This accounts for the rapid diminution in adsorption between 800 and 1000 °C. It also points out

that considerable fine tuning of small-molecule transport may be found by controlling the time and final temperature of annealing in this temperature regime.

One of the most important but unanticipated results of this study is the observation of nanostructures in the 1200 °C material that strongly resemble the onion-skin fullerenes reported by Iijima and Ugarte.[35−39] One reason that this morphological feature is surprising to find, is that the pathway from the polymer via pyrolysis to this structure is seemingly so dissimilar from the pathway via graphite electrode vaporization. Perhaps, at 1200 °C in these experiments, there is an approach to conditions resembling the cooler region of the graphite electrode.

Finally, and perhaps most significantly, we have measured a process of symmetry breaking and pattern formation at the nanoscale that gives rise to the structural evolution of CMS. By examining this processing in more detail, one may be able to begin to control and, possibly, to direct with the course of carbon structure development. Ultimately, this mechanistic approach, combined with a fresh look at the relevant aspects of fullerene formation and structure, could lead to the preparation of crystalline forms of CMS resembling zeolites. That such materials have been anticipated already theoretically and one has been calculated to be more stable than C_{60}, adds real impetus to this line of research.[40]

Acknowledgment. S.J.B. would like to acknowledge the Alfred P. Sloan Foundation for support. Part of this work used IPNS at Argonne National Laboratory which is funded by the U.S. DOE, BES-Materials Science, under Contract W-31-109-ENG-38. The authors would like to thank Dr. Theodore A. Nolan, Manager of the Materials Analysis User Center, for facilitating the microscopy research conducted at ORNL. Additional support for travel and direct access to the microscopy facilities at ORNL was provided by the Oak Ridge Institute for Science and Education (ORISE) and the Department of Energy, Assistant Secretary for Energy Efficiency and Renewable Energy, Office of Transportation Technologies, as part of the High Temperature Materials Laboratory User Program, under Contract DE-AC05-84OR211400 with Martin Marietta Energy Systems, Inc. (a division of Lockheed Martin).

CM960085W

(35) Ugarte, D. *Nature (London)* **1992**, *359*, 707.
(36) Ugarte, D. *Chem. Phys. Lett.* **1993**, *207*, 473.
(37) Iijima, S. *MRS Bull.* **1993**, *29*, 43.
(38) Ugarte, D. *MRS Bull.* **1993**, *29*, 39.
(39) Ugarte, D. *Carbon* **1995**, *33*, 989.
(40) Townsend, S. J.; Lenonsky, T. J.; Muller, D. A.; Nichols, C. S.; Elser, V. T. *Phys. Rev. Lett.* **1992**, *69*, 921.